nature medicine

Clinical translation of a high-performance neural prosthesis

Vikash Gilja[1–4,14], Chethan Pandarinath[1,2,5,14], Christine H Blabe[1], Paul Nuyujukian[1,2,5], John D Simeral[3,6–8], Anish A Sarma[3,6–8], Brittany L Sorice[8], János A Perge[3,6,7], Beata Jarosiewicz[6,7,9], Leigh R Hochberg[3,6–8,10], Krishna V Shenoy[2,5,11–13,15] & Jaimie M Henderson[1,5,15]

Neural prostheses have the potential to improve the quality of life of individuals with paralysis by directly mapping neural activity to limb- and computer-control signals. We translated a neural prosthetic system previously developed in animal model studies for use by two individuals with amyotrophic lateral sclerosis who had intracortical microelectrode arrays placed in motor cortex. Measured more than 1 year after implant, the neural cursor-control system showed the highest published performance achieved by a person to date, more than double that of previous pilot clinical trial participants.

Clinical trials have recently demonstrated that people with paralysis can control computer cursors and/or robotic limbs using neural prostheses that interpret neural signals acquired from chronically implanted cortical microelectrodes[1–4], scalp electroencephalography electrodes[5], or cortical surface electrocorticography electrodes[6]. Early studies with nonhuman primates (NHPs)[7–10] guided the initial development of neural prostheses, and prosthetic performance in NHPs continues to advance[11–16]. In the clinical domain, increasing neural prosthetic performance is crucial to moving beyond proof-of-concept into widespread adoption, and thus it is imperative to understand whether and how these advances in animal models will translate to clinical populations. Through studies in NHPs, we recently developed a high-performance neural prosthesis that outperformed existing demonstrations of neural cursor-control[15]. In this report we describe the translation of that system, as part of the BrainGate2 multi-site pilot clinical trial (CAUTION: Investigational device. Limited by federal law to investigational use.), for use by two individuals (participants T6 and T7) with amyotrophic lateral sclerosis (ALS). Using this system, participants T6 and T7 achieved the highest-reported neural cursor-control performances to date by a person, as measured by the time required to acquire virtual targets.

Participants T6 and T7 completed the same cursor-control tasks that were previously completed by BrainGate2 participant S3 (ref. 17), which represents the highest previously published cursor-control performance in the BrainGate2 trial and, to our knowledge, represents the highest human neural cursor-control performance published to date (**Supplementary Table 1**). Relative to the system used by participant S3, the current neural prosthesis (**Fig. 1a**) integrates design choices for four critical components that have demonstrated the potential to increase performance: (i) system architecture on which the neural prosthesis is implemented, (ii) signal conditioning methods applied to measured electrophysiological signals, (iii) a decoding algorithm that maps neural activity to movement intentions and (iv) a choice of behavioral actions associated with cursor-control. Below we outline each of these components.

The current neural prosthesis was built on a real-time hardware and software platform designed to reduce latency and jitter from hundreds of milliseconds (S3 study)[17] to 20 ± 6 ms. This advance was motivated by our previous NHP studies, which demonstrated that performance substantially increases with lower latency[18], and which used an earlier version of this platform to achieve high-performance neural control in NHPs[15,16].

The signal-conditioning stage, which extracts neural spike event and local field potential features from recorded electrode voltage potentials in real time, was modified to better adapt to the challenges of the clinical study environment (the participants' homes). These settings had considerably more electromagnetic noise than a controlled laboratory environment, which could potentially obscure the features of interest. To compensate, common average referencing[1,19] and phase-preserving filtering[1,20,21] were used to better separate neural spikes and local field potentials from background noise. In the previous study (of participant S3)[17], spikes were extracted by thresholding the spikeband (high-pass filtered) signal from each recording channel and sorting these waveforms into putative single neural units. In contrast, the current study (of participants T6 and T7) used simpler threshold-crossing counts as neural features. These features demonstrated nearly equivalent decoding performance and the potential for greater stability in NHP studies[22,23], and they were used in a previous clinical study[1].

In the current study, we use the Recalibrated Feedback Intention Trained Kalman Filter (ReFIT) decoding algorithm instead of the Velocity Kalman Filter (VKF) decoding algorithm previously used in the S3 study[17]. In a previous NHP study, we demonstrated that ReFIT outperforms VKF[15].

[1]Department of Neurosurgery, Stanford University, Stanford, California, USA. [2]Department of Electrical Engineering, Stanford University, Stanford, California, USA. [3]School of Engineering, Brown University, Providence, Rhode Island, USA. [4]Department of Electrical and Computer Engineering, University of California San Diego, La Jolla, California, USA. [5]Stanford Neurosciences Institute, Stanford University, Stanford, California, USA. [6]Center for Neurorestoration and Neurotechnology, Rehabilitation R&D Service, Department of Veterans Affairs Medical Center, Providence, Rhode Island, USA. [7]Brown Institute for Brain Science, Brown University, Providence, Rhode Island, USA. [8]Department of Neurology, Massachusetts General Hospital, Boston, Massachusetts, USA. [9]Department of Neuroscience, Brown University, Providence, Rhode Island, USA. [10]Neurology, Harvard Medical School, Boston, Massachusetts, USA. [11]Department of Neurobiology, Stanford University, Stanford, California, USA. [12]Department of Bioengineering, Stanford University, Stanford, California, USA. [13]Howard Hughes Medical Institute, Stanford University, Stanford, California, USA. [14]These authors contributed equally to this work. [15]These authors jointly directed this work. Correspondence should be addressed to J.M.H. (henderj@stanford.edu).

Received 21 November 2014; accepted 26 August 2015; published online 28 September 2015; doi:10.1038/nm.3953

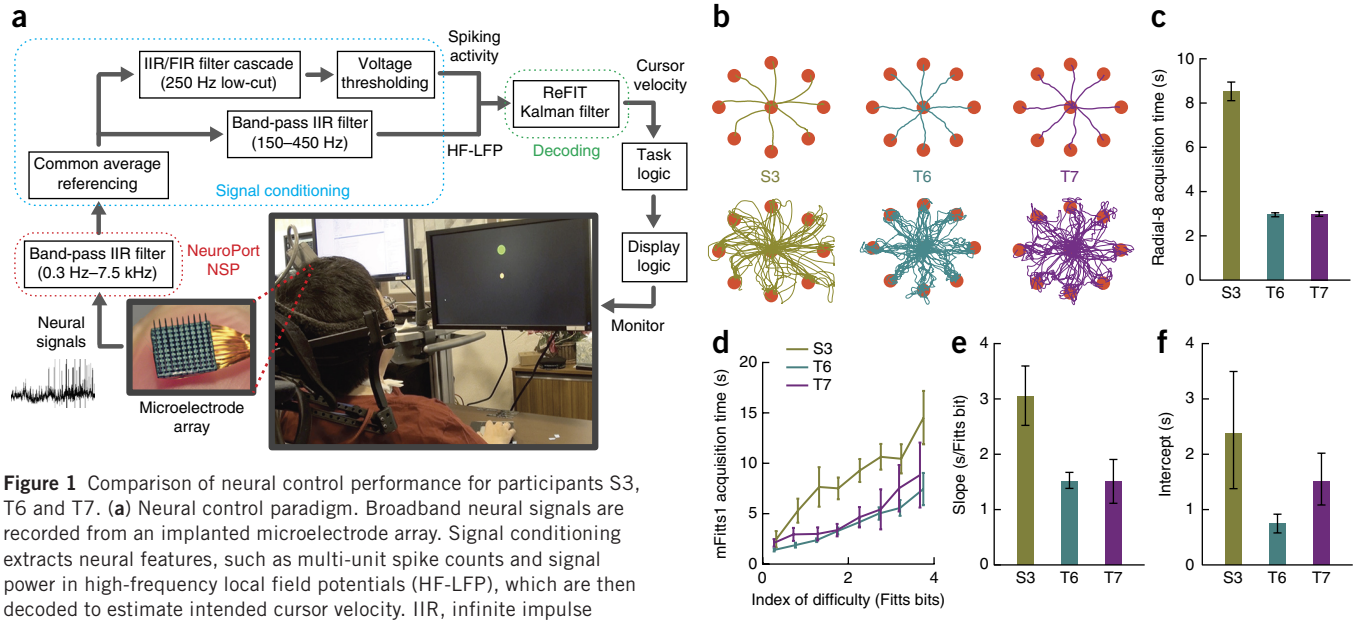

Figure 1 Comparison of neural control performance for participants S3, T6 and T7. (**a**) Neural control paradigm. Broadband neural signals are recorded from an implanted microelectrode array. Signal conditioning extracts neural features, such as multi-unit spike counts and signal power in high-frequency local field potentials (HF-LFP), which are then decoded to estimate intended cursor velocity. IIR, infinite impulse response; FIR, finite impulse response. (**b**) Radial-8 cursor trajectories. Top, mean trajectories of 15 randomly selected trials per target; bottom, 10 randomly selected example trajectories per target. (**c**) Target-acquisition time (mean ± 95% bootstrap confidence intervals) for Radial-8 (S3: 278 trials, T6: 665 trials, T7: 358 trials). Acquisition times for participants T6 and T7 are significantly lower than those for participant S3 ($P < 10^{-100}$, unpaired *t*-test). (**d**) mFitts1 performance summary (S3: 248 trials, T6: 1,072 trials, T7: 241 trials): index of difficulty was binned at 0.5-bit intervals and mean target-acquisition times (mean ± 95% confidence intervals) were calculated. (**e**,**f**) Slope (**e**) and intercept (**f**) for linear regression of index of difficulty versus acquire time for mFitts1 (95% bootstrap confidence intervals). Acquisition times for participants T6 and T7 are significantly lower than those for participant S3 ($P < 1 \times 10^{-5}$, analysis of covariance). Acquisition times for participants T6 and T7 include the 500-ms dwell time used by these participants to select targets. Sessions shown are 224–256 and 349–387 d after implantation for participants T6 and T7, respectively (participant T6 achieved comparable performance when tested 628, 791 and 798 d after implantation (**Supplementary Table 2**)). Data from participant S3 in **b**–**e** are re-plotted with author permission from ref. 17. Values plotted in this figure are summarized in **Supplementary Table 3**.

The decoding algorithm is typically calibrated with data in which the participant is either imagining or attempting specific movements. For participant S3, data from imagined wrist movements were used[17]. In the current study, participants performed (T6) or attempted (T7) finger movements, instead of arm or wrist movements, based on offline analyses demonstrating that actual or attempted finger movements were accompanied by neural activity that was more robustly decoded into cursor movements (**Supplementary Fig. 1**).

Participants T6 and T7 repeated two cursor-control tasks previously completed by participant S3. The first task, 'Radial-8', presented fixed-size targets that alternated between the center of the workspace and one of eight peripheral locations (**Fig. 1b**; **Supplementary Videos 1** and **2**). To successfully acquire a target, participants T6 and T7 held the cursor on the target for 500 ms, in contrast to participant S3, who supplied a neurally derived 'click' signal when on target. Participants T6 and T7 were able to successfully acquire and hold peripheral targets in less than half the time required by participant S3 (**Fig. 1c**; see **Supplementary Fig. 2** for further quantification and visualization). To assess the generalizability of this reduction in target-acquisition time, we also compared performance in the more-complex 'mFitts1' target-acquisition task. This task used variable-sized targets that appeared at pseudorandom directions and distances from the previous target (**Supplementary Videos 1** and **2**). Thus, mFitts1 assessed target-acquisition time across a range of target difficulties. Mean acquisition times suggest higher performance for participants T6 and T7 relative to that for participant S3 (**Fig. 1d**).

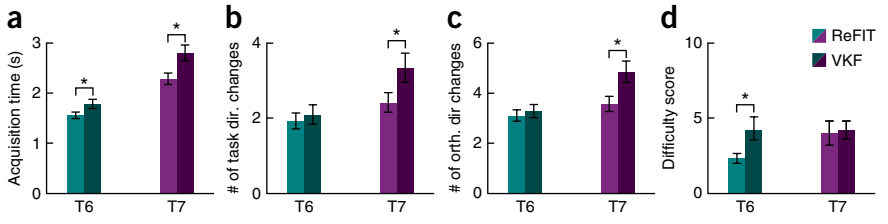

Figure 2 Comparison of VKF and ReFIT neural control performance for T6 and T7. (**a**) Target acquisition time, including the 500-ms dwell time (performance for individual blocks shown in **Supplementary Fig. 8a**,**b**). (**b**,**c**) Two additional performance measures that are relative to the task movement axis, defined by the line that intersects the center of the cursor at the start of the trial and the center of the target. (**b**) Task direction change count is the number of times the cursor velocity in the task movement axis reversed signs. (**c**) Orthogonal direction change count is the number of times the cursor velocity orthogonal to the task movement axis reversed signs. Data in panels **a**–**c** represent 418 (VKF) and 377 (ReFIT) trials for participant T6, and 418 (VKF) and 555 (ReFIT) trials from participant T7. (**d**) Participant-reported difficulty scores within a range of zero (effortless control) to ten (impossible control). Data represent four comparison blocks (participant T6) and five comparison blocks (participant T7) for each decoder (individual ratings are shown in **Supplementary Fig. 8c**). For all bar graphs, the mean ± 95% bootstrap confidence intervals are shown and the asterisk (*) indicates a significant difference between VKF and ReFIT (*$P < 0.01$, unpaired *t*-test). Values plotted in this figure are summarized in **Supplementary Table 4**. Channel counts used by each decoder are summarized in **Supplementary Table 5**.

As in previous studies[17], mFitts1 performance was summarized using a linear regression between target difficulty and acquisition time (**Fig. 1e**,**f**; **Supplementary Figs. 3** and **4**). The average regression intercepts for participants T6 and T7 were less than those of participant S3, suggesting a reduction in minimum acquisition time. More importantly, the regression slopes for participants T6 and T7 were significantly lower than those of participant S3 (95% bootstrap confidence intervals), indicating a smaller acquisition-time penalty as target difficulty is increased.

One potential real-world functional use of a neural prosthetic system for people with motor impairment is free-choice, free-paced typing[24]. We tested our neural prosthetic system in such an application with participant T6 using the Dasher assistive typing interface[25]. This software package (commonly used with physical interfaces such as eye-gaze trackers) maps two-dimensional cursor-control onto discrete typing, and it optimizes letter presentation on the basis of letter occurrence probabilities. Participant T6, who had previous Dasher interface experience, was able to use our neural prosthetic system to free-type 115 words in <19 min, or approximately six words per minute (**Supplementary Fig. 5** and **Supplementary Video 3**).

The ReFIT decoding algorithm used by participants T6 and T7 was previously developed in NHP studies as refinements to the VKF decoding algorithm[15], building on previous VKF-based studies with NHPs and humans[17,26]. To assess the specific contribution of the ReFIT decoder algorithm innovations on cursor-control in the present study, we directly compared VKF and ReFIT in a block design in which participants were unaware of which control algorithm was used (**Fig. 2**). Analogously to the previous NHP study and the Radial-8 task, participants performed a center-out-and-back task. Task parameters (target size, target distance and maximum trial duration) were chosen to facilitate a high success rate with VKF decoder control and were held constant for both VKF and ReFIT decoder control blocks. On average, ReFIT decoder algorithm-based target acquisition was significantly faster than VKF-based target acquisition (**Fig. 2a**). These findings are consistent with relative performance improvements measured in a previous BrainGate2 study comparing similar algorithmic innovations[27].

Participant T7 made fewer movement direction and orthogonal direction changes (**Fig. 2b**,**c**) during ReFIT decoder control blocks, indicative of improved path quality relative to VKF decoder control. These differences were not significant for participant T6. However, subjective self-reporting suggests that participant T6 expended cognitive effort to compensate for relative difficulties in VKF control. After each block, participants rated control difficulty on a scale from zero to ten, with zero defined as no effort (cursor automatically moved to the target) and ten defined as impossible. Participant T6 rated ReFIT decoder blocks as significantly easier (**Fig. 2d**, $P < 0.01$). When asked for a qualitative description of the cursor-control experience, participant T6 often commented that blocks that were rated as having a higher level of difficulty required a cognitive strategy, such as visualizing a 'ruler between the cursor and target' or imagining 'a gravitational force around the target.' For VKF decoder blocks, participant T6 also mentioned trying to slow down cursor movements to avoid overshooting the target. (In the NHP study, the presence of these overshoots was a differentiating feature between VKF and ReFIT, and it contributed substantially to the longer acquisition times we found with VKF[15].) In contrast to VKF, participant T6 often described ReFIT-based control as 'intuitive.' These results suggest that future animal and human studies should address the roles of cognitive load and strategies in neural prosthetic control, perhaps by incorporating cognitive distractors in task designs and assessing cursor-control performance degradation.

Beyond the described design choices in system architecture, algorithms and behavioral instructions to the participants, other factors may contribute to the higher performance demonstrated by participants T6 and T7 relative to participant S3 and previous BrainGate2 study participants. Differences in electrophysiological recording quality were unlikely to have contributed; the recording quality of participant S3's array at the time of the comparison study[17] was similar to or better than that of participant T6 (**Supplementary Fig. 6**). One potential factor is the etiology of motor impairment; participant S3 has motor impairment as a result of brainstem stroke, whereas participants T6 and T7 were diagnosed with ALS. Although comparisons with prior studies suggest that performance is relatively independent of etiology (**Supplementary Table 1**), there is currently insufficient data to explore the relationship between specific motor disorders and neural prosthetic control. Another potential factor is the degree of motor ability. Although all three participants had intact sensory pathways, participant S3 was not capable of functionally relevant arm movement. Participant T7 retained limited and inconsistent finger movements, and participant T6 was capable of dexterous finger movements. To control for movement itself as a potential contributing factor to improved performance in participants T6 and T7, we conducted control sessions in which participant T6 actively suppressed her arm and hand movements. The resulting cursor-control performance was similar to that observed in sessions in which she did not suppress movements (**Supplementary Table 2** and **Supplementary Fig. 7**), suggesting that movement itself does not improve performance. Furthermore, although participant T7 had limited motor abilities relative to those of participant T6, both participants achieved similar cursor-control performance in these tests. Last, for all three participants, multiple factors that were not explored in these studies might have affected performance, such as the overall amount of gain and smoothing applied to the cursor velocity. Of course, other potential differences between participants could also lead to performance variation, as is the case with able-bodied individuals performing skilled motor tasks (for example, playing sports or musical instruments).

In this study, insights from NHP studies and recent clinical trials were applied to the design of a neural prosthetic system, resulting in higher-performance neural cursor control than had previously been measured. The continued translation of neural prosthetic system studies from animal models to clinical research is vital both for advancing system performance and for understanding real-world challenges. The incorporation of advanced, high-performance system design innovations, informed and iterated through clinical research, may bring neural prostheses closer to clinical utility for people with motor impairments.

METHODS

Methods and any associated references are available in the online version of the paper.

Note: Any Supplementary Information and Source Data files are available in the online version of the paper.

ACKNOWLEDGMENTS

The authors would like to thank participants T6, T7, S3 and their families; E.N. Eskandar for participant T7's implantation surgery; B. Davis, B. Pedrick, M. Coburn, B. Travers and D. Rosler for administrative support; S.I. Ryu for surgical assistance; L. Barefoot, P. Gigante, A. Sachs, S. Cash, J. Menon and S. Mernoff for clinical assistance; K. Newell for data collection assistance;

J. Saab and N. Schmansky for technical assistance; and J.P. Donoghue for helpful scientific discussions. This work was supported by the Stanford Institute for Neuro-Innovation and Translational Neuroscience; Stanford BioX-NeuroVentures; the Stanford Office of Postdoctoral Affairs; the Garlick Foundation; the Craig H. Neilsen Foundation; The US National Institutes of Health: the National Institute on Deafness and Other Communication Disorders (NIDCD) (R01DC009899, principal investigator (PI): L.R.H.; R01DC014034, PI: J.M.H.), the National Institute of Neurological Disorders and Stroke (NINDS) (RO1NS066311-S1, PI: K.V.S.), the Eunice Kennedy Shriver National Institute of Child Health and Human Development (NICHD)-National Center for Medical Rehabilitation Research (NCMRR) (N01HD53403 and N01HD10018, Sub-award PI: L.R.H.); the Rehabilitation Research and Development Service, Department of Veterans Affairs (B6453R and B6310N, PI: L.R.H.); and the Massachusetts General Hospital (MGH)-Deane Institute for Integrated Research on Atrial Fibrillation and Stroke. The content of this paper is solely the responsibility of the authors and does not necessarily represent the official views of the US National Institutes of Health, the Department of Veterans Affairs or the United States Government.

AUTHOR CONTRIBUTIONS

V.G. and C.P. were responsible for study design, further guided by K.V.S., J.M.H. and L.R.H. V.G. and C.P. were responsible for research infrastructure development, data collection, analysis, algorithm design and manuscript preparation. All authors contributed to the manuscript. P.N. and B.J. contributed to infrastructure development and algorithm design. C.H.B. and B.L.S. contributed to the data collection effort from study participants T6 and T7, respectively. C.H.B. participated in study design. A.A.S. and J.D.S. contributed to infrastructure development. J.D.S. provided data from subject S3. J.A.P. and B.J. conducted offline analyses to inform algorithm design. J.M.H. was responsible for surgical implantation for study participant T6. L.R.H. is the sponsor-investigator of the multi-site pilot clinical trial. J.M.H. and K.V.S. were involved in all aspects of the study.

COMPETING FINANCIAL INTERESTS

The authors declare competing financial interests: details are available in the online version of the paper.

1. Hochberg, L.R. *et al. Nature* **485**, 372–375 (2012).
2. Hochberg, L.R. *et al. Nature* **442**, 164–171 (2006).
3. Collinger, J.L. *et al. Lancet* **381**, 557–564 (2013).
4. Aflalo, T. *et al. Science* **348**, 906–910 (2015).
5. Wolpaw, J.R. & McFarland, D.J. *Proc. Natl. Acad. Sci. USA* **101**, 17849–17854 (2004).
6. Wang, W. *et al. PLoS ONE* **8**, e55344 (2013).
7. Serruya, M.D., Hatsopoulos, N.G., Paninski, L., Fellows, M.R. & Donoghue, J.P. *Nature* **416**, 141–142 (2002).
8. Velliste, M., Perel, S., Spalding, M.C., Whitford, A.S. & Schwartz, A.B. *Nature* **453**, 1098–1101 (2008).
9. Taylor, D.M., Tillery, S.I. & Schwartz, A.B. *Science* **296**, 1829–1832 (2002).
10. Carmena, J.M. *et al. PLoS Biol.* **1**, e42 (2003).
11. Ganguly, K. & Carmena, J.M. *PLoS Biol.* **7**, e1000153 (2009).
12. Suminski, A.J., Tkach, D.C., Fagg, A.H. & Hatsopoulos, N.G. *J. Neurosci.* **30**, 16777–16787 (2010).
13. Mulliken, G.H., Musallam, S. & Andersen, R.A. *J. Neurosci.* **28**, 12913–12926 (2008).
14. Bensmaia, S.J. & Miller, L.E. *Nat. Rev. Neurosci.* **15**, 313–325 (2014).
15. Gilja, V. *et al. Nat. Neurosci.* **15**, 1752–1757 (2012).
16. Sussillo, D. *et al. J. Neural Eng.* **9**, 026027 (2012).
17. Simeral, J.D., Kim, S.P., Black, M.J., Donoghue, J.P. & Hochberg, L.R. *J. Neural Eng.* **8**, 025027 (2011).
18. Cunningham, J.P. *et al. J. Neurophysiol.* **105**, 1932–1949 (2011).
19. Perge, J.A. *et al. J. Neural Eng.* **11**, 046007 (2014).
20. Quian Quiroga, R. *J. Neurosci. Methods* **177**, 194–198 (2009).
21. Masse, N.Y. *et al. J. Neurosci. Methods* **236**, 58–67 (2014).
22. Fraser, G.W., Chase, S.M., Whitford, A. & Schwartz, A.B. *J. Neural Eng.* **6**, 055004 (2009).
23. Christie, B.P. *et al. J. Neural Eng.* **12**, 016009 (2015).
24. Bacher, D. *et al. Neurorehabil. Neural Repair* **29**, 462–471 (2015).
25. Ward, D.J. & MacKay, D.J. *Nature* **418**, 838 (2002).
26. Kim, S.P., Simeral, J.D., Hochberg, L.R., Donoghue, J.P. & Black, M.J. *J. Neural Eng.* **5**, 455–476 (2008).
27. Jarosiewicz, B. *et al. J. Neural Eng.* **10**, 046012 (2013).

ONLINE METHODS

Permissions. Permission for these studies was granted by the US Food and Drug Administration (Investigational Device Exemption) and the Institutional Review Boards of Stanford University, Partners Healthcare/Massachusetts General Hospital and the Providence VA Medical Center. The three participants in this study, T6, T7 and S3, were enrolled in a pilot clinical trial of the BrainGate Neural Interface System (ClinicalTrials.gov Identifier: NCT00912041).

Participants. Participants were included by following the inclusion and exclusion criteria of the clinical trial, and informed consent was obtained from all participants. Consent to publish photos of participant T6 was obtained from participant T6.

Participant T6 is a right-handed woman, 51 years old at the start of the study, who was diagnosed with ALS and had resultant motor impairment (functional rating scale (ALSFRS-R) measurement of 16). In December 2012, a 96-channel intracortical silicon microelectrode array (1.0-mm electrode length, Blackrock Microsystems, Salt Lake City) was implanted in the hand area of dominant motor cortex as previously described[17,28]. T6 retained dexterous movements of the fingers and wrist (see 'Neural control algorithms'). Data reported in this study are from T6's trial days 151, 161, 224, 228, 245, 256, 270, 628, 791 and 798. On all trial days, T6 achieved 94% or higher success rates for each control or task type reported. The typing video is from trial day 270.

The second study participant, T7, was a right-handed man, 54 years old at the time of the study, who was diagnosed with ALS and had resultant motor impairment (ALSFRS-R of 17). Participant T7 had two 96-channel intracortical silicon microelectrode arrays (1.5-mm electrode length, Blackrock Microsystems) implanted in the hand area of dominant motor cortex. T7 retained limited finger movements (see 'Neural control algorithms'). Data reported are from T7's trial days 349, 363, 378 and 387. On all trial days, T7 achieved 86% or higher success rates for each control/task type reported.

All data sets collected were included in analyses except for those from three sessions with participant T6. One session was excluded because of administration of a sedating medication unrelated to the clinical trial before the session. The second session was excluded because participant T6 self-identified as having deviated from session instructions. The third session was excluded because participant T6 was asked to suppress movement during neural control but deviated from these session instructions. Details of data collection from the third study participant, S3, are previously described[17].

Task design. Participants engaged in center-out-and-back and random point-to-point target-acquisition tasks. Cursor velocities were controlled using a neural control algorithm (described below). Targets were acquired by moving the cursor and holding it over the target for 500 ms.

For the center-out-and-back tasks, fixed size targets alternated between the center of the screen and one of eight locations on the periphery. The center-out-and-back task was set up with two different sets of target configurations. For performance comparisons to previous trial participant S3, target sizes and distances were scaled to match those described previously as task parameters for the Radial-8 task[17]. Radial-8 data presented are from test blocks T6-D224-B9/B10, T6-D228-B10, T6-D245-B23, T6-D256-B10, T7-363-B6/B8, T7-D387-B5/B7 (participant-trial day-block number), composed of 665 and 358 trials from T6 and T7, respectively.

To compare VKF and ReFIT performance, target sizes were increased to permit a high success rate for both VKF and ReFIT based control to facilitate direct comparison of time to target and cursor trajectories. VKF data are from test blocks T6-D151-B6/B9/B13, T6-D161-B3/B5, T7-D349-B17, T7-D363-B11, T7-D378-B105/B108/B110, composed of 418 and 418 trials from T6 and T7, respectively. ReFIT data are from test blocks T6-D151-B8/B12/B15, T6-D161-B4, T7-D349-B18, T7-D363-B12, T7-D378-B104/B106/B109, composed of 377 and 555 trials from T6 and T7, respectively. (Additional T6 data is summarized in **Supplementary Fig. 8a**, but was excluded from the analysis owing to a failure to successfully acquire targets using the VKF.)

The random point-to-point target-acquisition task was matched to the mFitts1 task previously run with participant S3 (ref. 17). In this task, target size was chosen psuedorandomly from three fixed diameters. Subsequent target directions and distances were also chosen pseudorandomly, but they were adjusted to ensure that targets appeared fully within the computer monitor workspace.

For the mFitts1 task, Index of Difficulty for each trial was calculated as follows:

$$ID = \log_2((D/W)+1),$$

where D denotes distance from the cursor's start position to the closest edge of the acceptance window, W denotes the acceptance window (which is computed as the sum of the target diameter and the cursor radius). This formulation differs slightly from that specified in ref. 17 by including two provisions: first, a provision for the effective reduction in the distance to the target due to the size of the target and cursor, and second, a provision for the effective increase in the acceptance window due to the size of the cursor. This formulation allows for more robust comparison across a variety of task designs, as in ref. 15. The mFitts1results for participant S3 in **Figure 1d,e** were calculated using the above formulation for comparison to the current study. These data are from test blocks T6-D224-B8/B12, T6-D228-B11, T6-D245-B21, T6-D256-B14/B17, T7-D363-B5/B7, T7-D387-B4/B6, composed of 1,072 and 241 trials from T6 and T7, respectively.

Neural control algorithms. ReFIT and VKF decoding algorithms were previously described in detail in an NHP study[15]. Neural control was continuous throughout each test block. The real-time input to both control algorithms were neural features described below. As in the NHP study, algorithm parameters were calibrated with training data collected during the same research session as evaluation of neural control performance. All training data were collected with a center-out-and-back target configuration. VKF training data were collected with either motor-based control or automated open-loop control. ReFIT decoder training data were collected with VKF decoder based neural control.

In motor-based control (T6), the participant controlled the cursor's position by making physical movements with their index finger on a wireless touchpad (Magic Trackpad, Apple). T6 was not limited in her ability to span the workspace of the touchpad. Parameters of the VKF decoder in the T6 sessions reported in the main manuscript were calibrated with motor-based training data. For participant T7, early sessions attempted to use motor-based control to calibrate the VKF decoder. T7's movement ability was more limited, however, and maximally spanned a small region on the touchpad (~1/8–1/4 inches wide), resulting in poor kinematic data. For all T7 sessions reported, VKF decoder parameters were instead calibrated to automated open-loop training data, in which the cursor was automatically moved directly toward the target by the computer (as in ref. 17). The T6 sessions reported in **Supplementary Table 2** also used automated open-loop training data to calibrate VKF control algorithm parameters. Participants were asked to attempt (T7) or imagine (T6) finger-based movements for open-loop training. For both motor and open-loop control, the choice of finger-based movements was based on considering various contralateral arm and hand movements and choosing movements that elicited the most neural activity (detailed in **Supplementary Fig. 1**). The previous NHP study[15] associated cursor movements with compound arm movements by tracking end effector kinematics.

Neural control and task cueing were controlled by custom software run on the Simulink/xPC real-time platform (The Mathworks, Natick, MA), enabling millisecond-timing precision for all computations. Neural data collected by the NeuroPort System (Blackrock Microsystems, Salt Lake City) were available to the real-time system with 5-ms latency. Visual presentation was provided by a computer via a custom low-latency network software interface to Psychophysics Toolbox for MATLAB[29,30] and an LCD monitor with a refresh rate of 120 Hz. Frame updates from the real-time system occurred on screen with a latency of approximately 13 ± 5 ms.

Neural feature extraction and selection. The NeuroPort System applies an analog 0.3 Hz to 7.5 kHz band-pass filter to each neural channel and samples each channel at 30 kSamples per second. These broadband samples were processed via software on the Simulink/xPC real-time platform. The first step in this processing pipeline was to subtract a common average reference (CAR) from each channel[1,19,31]. For each sample, CAR was calculated by taking the

doi:10.1038/nm.3953

mean across all properly recorded neural channels (channels with outlier noise characteristics were not included). The CAR operation was intended to remove noise common across all recorded neural channels (for example, see the supplementary material in ref. 19).

Band-pass filters split the signal into spike and high frequency local field potential (HF-LFP) bands. HF-LFPs were used in combination with spikes (hybrid decoding) as HF-LFPs can contain valuable kinematic information not always accessible if signals are restricted to recorded spikes[19]. To extract neural spiking activity a cascaded infinite impulse response (IIR) and finite impulse response (FIR) high-pass filter was applied. Although the IIR filter efficiently provides a sharp high-pass cutoff, it introduces a phase distortion that reduces action potential discriminability from noise. Thus, an asymmetric FIR filter was designed to reduce the impact of this phase distortion[1,20,21]. A threshold detector was applied every millisecond to detect the presence of a putative neural spike. HF-LFP power features refer to the power within the 150–450-Hz band-pass filtered signal. The sessions with T6 and T7 reported in the main manuscript figures used only spike-based features. The T6 sessions reported in **Supplementary Table 2** and the Dasher control session used both spike and HF-LFP power features.

Neural features and spike thresholds were selected in session during parameter calibration. Neural features were sorted on the basis of their correlation to velocity control. Features were added one by one to the neural control algorithm and an offline assessment of directional control was used to predict online control quality (see the supplementary material in ref. 15). This process was repeated for multiple spike-detection threshold values, and the feature set selected was the one that achieved the minimum decoding error using the fewest number of channels. Neural feature values were updated with a fixed period during online control sessions. This period varied between 10–50 ms and was always matched between VKF and ReFIT.

For sessions with participant T7, neural features showed drifts in baseline rates over time. To account for these nonstationarities, baseline rates were computed *de novo* before each block, during a 30-s period in which the participant was asked simply to relax. In addition, baseline rates were continually updated over the course of the block using the following update equation:

$$b_{k,t} = b_{k,t-1} + (n_{k,t} - b_{k,t-1}) \times \frac{1}{\tau}$$

where $b_{k,t}$ denotes the estimated baseline rate of feature k at time t, $n_{k,t}$ denotes the instantaneous rate for feature k at time t, and τ is the adaptation time constant (30 s). These estimated baseline rates were subtracted from the instantaneous rates before being passed into the decoding algorithms. Further, to minimize the number of terms that could be impacted by nonstationarities, the position feedback component of the ReFIT algorithm (detailed in ref. 15) was removed for participant T7. Both modifications (baseline tracking and removal of position feedback) were also evaluated with participant T6 in the sessions reported in **Supplementary Table 2**.

Code availability. Code may be made available upon request to the corresponding author.

28. Kim, S.-P. *et al. IEEE Trans. Neural Syst. Rehabil. Eng.* **19**, 193–203 (2011).
29. Pelli, D.G. *Spat. Vis.* **10**, 437–442 (1997).
30. Brainard, D.H. *Spat. Vis.* **10**, 433–436 (1997).
31. Chestek, C.A. *et al. J. Neural Eng.* **10**, 026002 (2013).